

2 **Joint assembly and genetic mapping of the Atlantic horseshoe crab**
3 **genome reveals ancient whole genome duplication.**

4 Carlos Nossa¹, Paul Havlak¹, Jia-Xing Yue¹, Jie Lv¹, Kim Vincent¹, H Jane Brockmann³, Nicholas
5 H Putnam^{1,2}

6 (1) Department of Ecology and Evolutionary Biology, and (2) Department of Biochemistry and Cell
7 Biology, Rice University, P.O. Box 1892, Houston TX 77251-1892; (3) Department of Biology, P.O.B. 11-
8 8525, University of Florida, Gainesville, FL 32611-8525.

Address for correspondence:

9 nputnam@rice.edu

10 Nicholas Putnam
11 Ecology and Evolutionary Biology – MS 170
12 Rice University
13 P.O. Box 1892
14 Houston, TX 77251-1892

15 Keyword: Genotyping-by-Sequencing (GBS)

16 Keyword: Genetic linkage mapping

17 Keyword: Genome evolution

18 Keyword: Limulus polyphemus

Abstract

Horseshoe crabs are marine arthropods with a fossil record extending back approximately 450 million years. They exhibit remarkable morphological stability over their long evolutionary history, retaining a number of ancestral arthropod traits, and are often cited as examples of “living fossils.” As arthropods, they belong to the *Ecdysozoa*, an ancient super-phylum whose sequenced genomes (including insects and nematodes) have thus far shown more divergence from the ancestral pattern of eumetazoan genome organization than cnidarians, deuterostomes, and lophotrochozoans. However, much of ecdysozoan diversity remains unrepresented in comparative genomic analyses. Here we use a new strategy of combined *de novo* assembly and genetic mapping to examine the chromosome-scale genome organization of the Atlantic horseshoe crab *Limulus polyphemus*. We constructed a genetic linkage map of this 2.7 Gbp genome by sequencing the nuclear DNA of 34 wild-collected, full-sibling embryos and their parents at a mean redundancy of 1.1x per sample. The map includes 84,307 sequence markers and 5,775 candidate conserved protein coding genes. Comparison to other metazoan genomes shows that the *L. polyphemus* genome preserves ancestral bilaterian linkage groups, and that a common ancestor of modern horseshoe crabs underwent one or more ancient whole genome duplications (WGDs) ~300 MYA, followed by extensive chromosome fusion.

Introduction

38 Comparative analysis of genome sequences from diverse metazoans has revealed much about
40 their evolution over hundreds of millions of years. The discovery of extensive gene homology
42 across large evolutionary distances has allowed researchers to track chromosome rearrangements
and whole genome duplications. The resulting value of whole chromosome sequences presents
a challenge for existing whole genome shotgun (WGS) assembly strategies.

44 Whole genome duplication events were long suspected[1], but only the availability of genome
46 sequences has allowed confirmation of them in fungal, vertebrate, plant, and ciliate lineages[2–5].
In contrast, when only a few chordate, insect, and nematode genomes were available, conserva-
48 tion of gene linkage (i.e. synteny) and gene order were observed only between closely-related
species, and consequently were not expected to be conserved between phyla. As more metazoan
genomes have been sequenced, it has become clear that long-range linkage has been conserved
over long time scales in many lineages.

50 Sequencing the genomes of representatives of chordate, mollusk, annelid, cnidarian, placo-
zooan and sponge clades has identified 17 or 18 ancestral linkage groups (ALGs)[6–10]. Each of
52 these ALGs consists of a set of ancestral genes whose descendants share conserved synteny
in multiple sequenced genomes. These ALGs have been interpreted to correspond to ances-
54 tral metazoan chromosomes, and correlations between inferred rates of gene movement between
ALGs across the metazoan tree suggest that these ancestral linkage relationships are conserved
56 through the action of selective constraints on a subset of genes[11].

58 The relatively small number of genomes from anciently distinct metazoan lineages and the
fragmented nature of draft genome assemblies still limit both the search for ancient whole genome
60 duplications and the power of the data to constrain models of chromosome-scale genome structure
evolution. While WGS sequencing technology and assembly methods are active areas of research
and technological development, and have improved at a dramatic pace in recent years, high quality
62 *de novo* assembly of large, complex metazoan genomes remains a difficult and resource-intensive
problem. Without genetic or physical maps, or reliance on a high-quality reference genome of a
64 closely-related species, WGS sequencing projects still typically produce assemblies containing
thousands of scaffolds, hundreds of scaffolds incorrectly joining sequence from different chromo-
66 somes, or both[12].

68 Next-generation sequencing has greatly reduced the cost of constructing high density genetic
maps by eliminating the need to develop and genotype polymorphic markers individually[13]. This
has been achieved either by focusing sequence coverage within or adjacent to genomic regions
70 of distinct biochemical character, such as restriction sites with RAD-seq and related methods[14,
15], or by combining information across regions using a reference genome sequence[16, 17].
72 While RAD-seq is applicable to organisms lacking a reference genome assembly, it is not directly
applicable to comparisons of genome organization across long evolutionary time spans because
74 such comparisons rely on the identification of homologous sequence markers (typically protein-
coding genes), which typically have only a small overlap with the restriction-associated markers.

76 Here we present a genotype-by-sequencing method for constructing a high-density genetic
map using low-coverage, low-cost, whole genome sequencing data from the offspring of a wild
78 cross. In this joint assembly and mapping (JAM) approach the traditionally independent and se-
quential steps of genome assembly, polymorphic marker identification, and genetic map construc-
80 tion are combined. Existing assemblers expect lower densities of sequence polymorphism, deeper
coverage, greater computer memory, or more aggressive quality trimming that decrease sequence
82 coverage[18–20]. Our current implementation focuses on conservative assembly of short scaffolds
sufficient for map construction, but our results suggest that further integration of genetic mapping

84 information within whole genome shotgun assembly methods can be a cost effective way to pro-
duce assemblies of large, complex genomes with chromosome-scale contiguity.

86 We have applied this approach to produce a genetic map of the genome of the Atlantic
horseshoe crab, *Limulus polyphemus*. Horseshoe crabs are marine arthropods with a fossil
88 record extending back ~450 million years[21]. They exhibit remarkable morphological stability
over their long evolutionary history, retaining a number of ancestral arthropod traits[22], and are
90 often cited as examples of “living fossils.” *L. polyphemus* has a large genome about 90% the size
of the human genome. It is an important species from ecological, commercial, and conservation
92 perspectives[23], that has been used as a model system for research in behavioral ecology, phys-
iology and development[24]. The map and SNP markers described here will be a resource for the
94 *L. polyphemus* genome project, research in horseshoe crab population biology, and comparisons
of metazoan genome organization. By anchoring protein coding genes to this map, we are able
96 to extend analysis of ancestral linkage groups and whole genome duplications to the chelicerate
lineage.

98 Results

Assembly and Mapping

100 The JAM method is designed to produce a combined assembly of polymorphic sequences, tagged
by genomic regions with at most one SNP per k -mer window (Methods). Starting with genomic
102 reads from a mating pair of adult *L. polyphemus* and 34 offspring (~100 bp reads on ~300 bp
inserts), we tabulated high-quality 23-mers occurring in two sequencing runs (and thus also in at
104 least two individuals).

Fitting Poisson models for unduplicated sequence to the frequencies of these filtered 23-mers
106 suggests that 1.1 billion genomic loci are unique at this resolution. Of these k -loci, 63 percent are
modeled as homozygous, 27 percent as paired major-minor alleles, and the remaining 10 percent
108 as tied allele pairs (Figure 1). The corresponding SNPs, if always at least 23 bases apart, would
be 1.6 percent of bases in the k -loci. Dividing the total number of filtered 23-mers by the modeled
110 homozygous depth of coverage $d = 38.9$ yields an estimated genome size of 2.74 billion bases,
consistent with the measured DNA content of 2.8 pg (978 Mb \simeq 1 pg DNA)[25].

112 We categorize specific 23-mers by their edit distances to others, having no neighbors within
a single base substitution (unique tags) or with a single mutually unique neighbor (“SNPmer pair”
114 tags). A subset of these, including SNPmer pairs for approximately 7.9 million SNPs, constitute
the tags used for contigging and scaffolding. The SNP-mer pairs account for about 45 percent of
116 the modeled fraction of alleles, the others missed from similarity to other sequences (e.g. due to
repeats) or distance from each other (because of indels or multiple SNPs per 23-mer).

118 Chaining these 23-mers together (see Methods) produces an initial 6.6 million contigs, 3.9
million of which are linkable by paired reads for scaffolding. Applying Bambus[26] produces 944
120 thousand scaffolds spanning 1.3 million bases (Table 1). These scaffolds serve as markers incor-
porating multiple k -loci, including SNPmer pairs used to identify haplotypes.

122 After assembly, the mean density of single nucleotide polymorphisms (SNPs) across the four
haplotypes in assembled regions was estimated based on read re-alignments to be 7.6 per thou-
124 sand bases. We jointly inferred the phases of these SNPs and segregation pattern (offspring
genotypes) in the mapping cross for each marker in a maximum likelihood framework (Methods).
126 We focused on the 91,320 markers with at least 18 inferred bi-allelic SNPs for constructing the link-
age map. These markers grouped into 1,908 high-confidence map bins (*i.e.* unique segregation

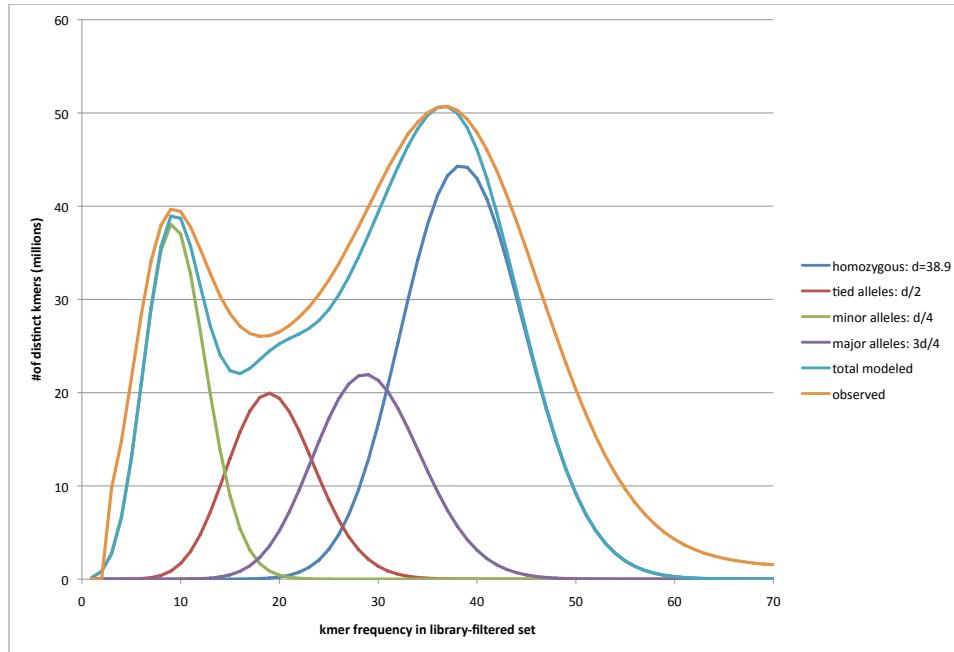


Figure 1: Fitting Poisson distributions to *Limulus* 23mer frequencies (filtered as described below)

128 patterns, assumed to correspond to loci in the genome uninterrupted by meiotic recombination in
 130 the cross[27]). Map bins fell into 32 linkage groups, close to the 26 pairs (2N=52) previously found
 132 in a cytogenetic analysis of two chromosome spreads[28]. 20 map bins were removed for having
 134 inconsistent positions in the maternal and paternal maps, and 12 were singletons.

132 To estimate the frequency of incorrect genotype calls as a function of the log likelihood dif-
 134 ference between the called and alternative genotype (genotype confidence score), including con-
 136 tributions from uncertainty in SNP-mer identification, assembly, and sampling noise, we carried
 138 out a simulation of the library pooling and sequencing, k -mer assembly and genotype inference
 140 protocols, using the sequenced *Ciona intestinalis* genome as a starting point.

138 In the simulated *C. intestinalis* data set (Methods), a single stretched exponential distribution
 140 provided a good fit to the frequency of genotype calling errors as a function of the call confidence
 142 score for scores up to 6, or down to error frequency of about 1%. The observed error frequency
 144 declined more slowly for higher confidence scores. The minimum χ^2 fit used for estimating the
 146 genotyping error rate in the *L. polyphemus* map bins was $p_e(s) = a_1 e^{-s^{c_1}/b_1} + a_2 e^{-s^{c_2}/b_2}$, with
 parameter values $a_1 = 0.49, b_1 = 2.08, c_1 = 1.26, a_2 = 5.47, b_2 = 0.17, c_2 = 0.16$ (Figure 2).

144 Applying this model to the *L. polyphemus* marker genome calls, we estimated that the genotype
 146 calling error rate in the map bin representative markers was 0.0099. 51% of adjacent map bin pairs
 are separated by a single inferred recombination event in the cross, and 94% are separated by
 three or fewer recombinants in each parent.

Of the 91,320 markers with at least 18 putative SNPs, 84,307 (92%) were assigned to their

Table 1: *K*-mer contig and scaffold statistics

Assembled	count	total (bp)	avg. span (bp)	n50 span (bp)
<i>k</i> -mer contigs	6,614,434	1,240,275,515	188	418
linkable contigs	3,925,844	1,137,576,911	290	460
initial scaffolds	944,246	1,261,263,172	1336	3047
reference scaffolds	944,246	1,295,334,515	1372	2930
reference bases		1,131,458,744	1198	2553

148 closest map bins with a threshold of $p < 10^{-6}$ (Methods), for an estimated genome-wide average
 150 density of one mapped sequence marker every 32 kb. A mean of 45 markers were mapped to
 152 each map bin, and the number of markers mapped was used to estimate the relative physical size
 of map bins. 46% of the scaffolds with 12-17 SNPs could be placed with the same threshold, for
 an additional 32,688 markers, or one marker every 23 kb.

154 The total length of the scaffolds assigned to map bins was 411 Mb, and they contained 2.67
 156 million bi-allelic SNPs assigned a phase with a posterior probability of at least 0.99. Of these, 72%
 were inferred to be unique to one of the four parental chromosomes. This is close to the 74%
 predicted under the finite sites neutral coalescent model given the observed SNP density[29].

Sequence composition and recombination rate

158 In the scaffolds longer than 1kb (mean length 2.9 kb), the *G/C* base content was 33.3 ± 2.8 per-
 160 cent, and the local relative frequency of CpG dinucleotides was bimodally distributed, with about
 30% of sequences exhibiting depletion of CpG. TpG and CpA dinucleotides were over-represented
 162 on average and their local densities negatively correlated with CpG density, suggesting ongoing
 germ-line CpG methylation for a fraction of the genome[30].

164 The mean maternal and paternal recombination rates were estimated to be 1.28 and 0.76 cen-
 timorgans per megabase respectively, consistent with expectation based on genome size[31]. We
 166 did not observe evidence of segregation distortion for any map bins. Estimated local recombina-
 tion rates in the two parents are correlated across the genome with and $r^2 = 7.1\%$; $p < 1e-29$, and
 the mean local recombination rate is correlated with local SNP density, $r^2 = 9.7\%$; $p < 1e-40$.

Ancestral linkage group conservation

168 34,942 scaffolds have significant sequence conservation with 10,399 predicted proteins of the tick
 170 *Ixodes scapularis*[32]. 6,246 of these hits formed reciprocal best pairs, of which 5,775 (92%) could
 be placed on the linkage map at a threshold of $p < 10^{-6}$. These were used as conserved markers for
 172 comparisons of genome organization. When linkage groups were divided into 108 non-overlapping
 bins of 1,000 markers, 52 had significant ($p < 0.05$, after Bonferroni correction for 1,944 pairwise
 174 tests) enrichment in shared orthologs (or “hit”) with at least one of eighteen ancestral chordate
 linkage groups[7]. A hidden Markov model segmentation algorithm[6] identified 40 breakpoints
 176 in ALG composition in the linkage groups. 72% of the genome is spanned by 53 intervening
 segments that hit one or (for eight of them) two ALGs (Figures 4 and 5). Each of the eighteen
 178 ancestral ALGs has at least one hit among the 45 segments with a unique hit to the ALGs.

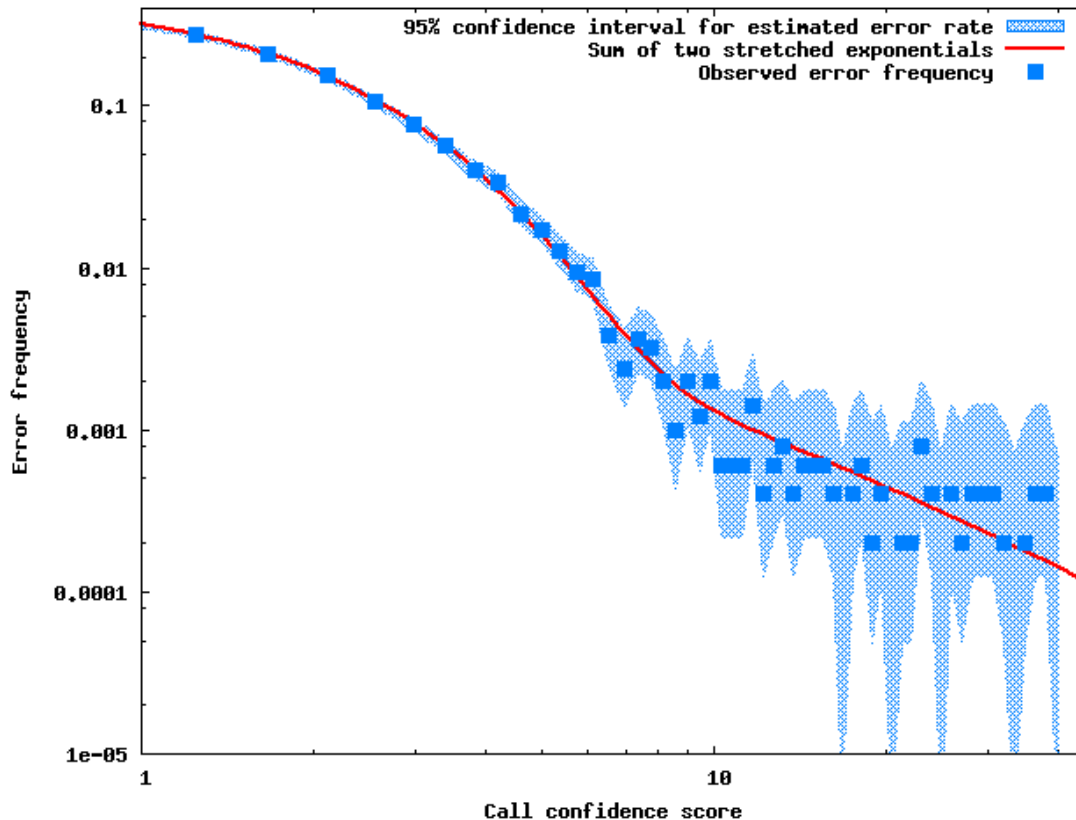


Figure 2: Genotype call error rate as a function of call confidence score for bins of 10,000 calls in simulated *Ciona intestinalis* genome data. The stippled blue region shows 95% confidence intervals of the Bayesian posterior probability distribution of the underlying error rate computed from the Beta distribution $\text{Beta}(n_e + 1, n_c - n_e + 1)$ conjugate the assumed binomial distribution of observed errors, where n_e and n_c are the number of errors and number of calls in each bin respectively.

Whole genome duplications

180 Whole genome duplication (WGD), or polyploidization is a rare but dramatic genetic mutation event
 182 which doubles the size of a genome and creates a redundant pair of copies from every gene. Be-
 184 cause it creates redundant copies of genes for entire biochemical pathways and genetic networks,
 it has been proposed that it creates unique raw material for the evolution of novel biological func-
 tions and increased complexity.

Homeobox gene clusters

186 Homeobox genes encode a large family of transcription factors involved in diverse embryonic pat-
 188 terning and structure formation processes of eukaryotes. As a particular subfamily of homeobox
 genes, the Hox cluster is known to control metazoan body patterning along the anterior-posterior
 190 axis. We identified 155 scaffolds with significant homology to predicted chelicerate homeobox
 gene sequences in public databases. We classified these sequences into homeobox subfamilies
 (Methods) and placed them on the map by best hit. Two large clusters of Hox genes are found

192 on linkage group (LG) 15 and LG 21, each containing multiple members of the anterior, central
194 and posterior classes. There are also two parahox cluster homologs, each with three homeobox
196 genes: *gsx* and *cdx* orthologs and a third homeobox gene not confidently assigned to a subfamily
in our analysis (LG 5 and LG 19). There are two smaller clusters containing multiple hox genes
(LG 18 and LG 20), and clusters of other homeobox genes, including members of the *msx*, *lhx*,
nk, *evx*, and *gbx* families (Figure 1).

198 Genomic distribution of paralogous genes

WGD creates many pairs of duplicate genes or “paralogs”. The distinctive features of these genes
200 have been used to infer WGD events in fungal, vertebrate and plant genomes[2–4]. We examined
the genomic distribution of 2,716 pairs of candidate paralogous gene markers in *L. polyphemus*
202 for signatures of WGD. In 45% of these pairs both markers mapped to the same chromosome,
compared to 5.3 ± 0.5 % in 1000 datasets with randomly-permuted paralogous gene identities.
204 The mapped positions of pairs within the chromosomes were highly correlated (average $r^2 = 0.81$,
and exceeding 0.95 for 8 of the large chromosomes; Figure 8), suggesting that many of the pairs
206 represent recent tandem gene duplicates or single genes fragmented across multiple markers. In
the following, these same-chromosome paralogs are referred to as “tandem” duplicates.

208 Inter-chromosomal duplicates are clustered into conserved paralogous micro-synteny blocks
(or “paralogons”[3]): there are 25 pairs of loci, each with at least six ($m_p = 6$) paralog pairs clustered
210 with a maximum gap (max-gap) of 300 markers between adjacent paralogs in each cluster. These
clusters span 25,044 markers, or 30% of the map, after removing redundancy from paralogons
212 with overlapping footprints. In 1000 datasets with randomly-permuted paralogous gene identities,
the maximum number of such clusters observed was 11; the mean and standard deviation were
214 3.9 ± 1.0 . The observed clustering into paralogons was greater than that in the randomized
datasets over a broad range of choices of max-gap and m_p . For example, for max-gap=100, m_p
216 =3 there are 52 clusters vs. 3.5 ± 1.9 , range 0-10; for max-gap=500, $m_p = 9$ there are 12 vs. 2.9
 ± 1.7 , range 0-9. Because of the large proportion of apparent tandem gene duplicates (45%), this
218 randomization scheme increases the number of inter-chromosomal paralog pairs relative to the
data, making it a conservative significance test for inter-chromosomal paralog clustering. When
220 genes with tandem duplicates are excluded from the randomizations, the observed number of
clusters is greater than the maximum observed in 1000 randomizations for all the combinations
222 of max-gap in the set (100, 200, 300, 400, 500, 600) and m_p in the set (3, 4, 5, 6, 7, 8, 9). 23
max-gap=600, $m_p = 7$ clusters span 59% of the map, compared to respective mean number and
224 map coverage of 3.3 ± 1.8 , and 13 ± 6 % in these randomizations.

226 Among the marker pairs mapping to different chromosomes, we find a significant excess of
pairs relating segments derived from the same ancestral linkage group (ALG) relative to random-
228 ization controls (247 pairs vs 102 ± 11 , $p < 0.001$ in randomizations of all genes; 202 vs 46 ± 7
when genes in tandem duplicates are excluded). This pattern is consistent with the creation of
these segments by duplication (rather than fission).

230 The max-gap clusters have a significant amount of overlap among their footprints. For example,
the footprints of the max-gap=600, $m_p = 7$ clusters had a total length of 72,072 markers, but a net
232 footprint after redundancy removal of 49,545 markers. We examined the relationships among the
paralogons for evidence of successive rounds of duplication. We considered a graph in which
234 nodes correspond to merged, non-redundant paralogon footprint regions. Nodes are connected
with edges if a max-gap cluster connects the two nodes. The average clustering coefficient of this
236 graph is equal to the probability that footprints a and c share a max-gap cluster, given that there
are edges (a, b) and (b, c) in the graph. We compared the clustering coefficients to those found in

238 random Erdős-Rényi graphs with the same number of nodes and edge probability as the observed
240 graph. We found that the observed data shows significantly more clustering than these random
242 graphs for a wide range of choices of max-gap and m_p . For example, for max-gap 600, $m_p = 7$,
the average clustering coefficient is 0.19, while 10,000 random graphs had coefficients of $0.034 \pm$
 0.042 , $p=0.0039$.

Age distribution of paralogous genes

244 Because WGD events create many paralogs at the same time, they leave characteristic peaks in
the age distribution of paralogous genes. In *L. polyphemus* the distribution shows peaks centered
246 at 0.71 and 1.34 substitutions per synonymous site (K_s), values within the approximately linear
response range of K_s estimates to WGD age[33] (Figure 9). For comparison, the synonymous site
248 divergence between an Asian horseshoe crab species *Tachypleus tridentatus* and *L. polyphemus*
has a mode of 0.35. The common ancestor of these species has been estimated to have lived
250 114-154 MYA, coincident with the opening of the Atlantic ocean[34], suggesting a WGD event
230-310 MYA, and possibly an older one 450-600 MYA.

Discussion

252 Our results demonstrate that a low cost, combined approach to whole genome sequencing and ge-
netic mapping can be used to efficiently create a very high density genetic recombination map for
254 a non-model organism with a large genome. Because the approach uses genome-wide sequenc-
ing, a large number of sequence markers can be anchored to the map, allowing comparisons of
256 genome organization at the chromosome scale over very large evolutionary divergences. The
identification of chromosomal segments with significant gene composition homology to each of
258 the chordate ALGs shows that the predominance of fusion and mixing of ancestral linkage groups
previously observed in analyzed ecdysozoan genomes[10] is not ancestral to or universal in the
260 clade.

262 The map allows quantitative characterization of other features of chromosome-scale organiza-
tion, such as the correlation between local recombination rate and polymorphism levels. Similar
264 positive correlations between local recombination rate and polymorphism level have been ob-
served in other metazoans including humans[35–37] and plants[38, 39]. Future comparisons to
266 more closely related chelicerates will allow tests to distinguish whether these rates are positively
correlated with inter-specific divergence, consistent with a neutral process of correlated mutation
268 and recombination rates[40]. Alternatively, the association could be explained by hitchhiking and
background selection[41].

270 The existence of duplicated hox and parahox clusters on four different chromosomes is highly
suggestive of multiple whole genome duplication. Hox clusters have not been found in duplicate
272 copies except in vertebrates where they have been created by whole genome duplication, and
have only rarely been subsequently lost.

274 The enrichment of inter-chromosomal paralog pairs in segments of the same ALG origin is
consistent with their creation by duplication (rather than fission), although because small-scale
276 duplication is biased toward local (tandem) duplication, fission of segments could also leave be-
hind an enrichment of paralogs. Such a mechanism, however, would not create the observed
278 organization of paralogs, *i.e.* their clustering into “paralogons”. The fact that these paralogons
span a large portion of the map (59%) suggests that it was a whole genome duplication, rather
280 than segmental duplications that have rise to the pattern.

282 The double-peaked shape of the distribution of synonymous site divergence between pairs
of paralogs, combined with the existence of two small clusters of HOX genes in addition to the
two complete HOX clusters suggests that there may have been two rounds of whole genome
284 duplication in the horseshoe crab lineage.

286 WGDs preceded major species radiations in vertebrates, angiosperms and teleost fish and the
importance of their role in evolution is the subject of long-running debate[2–4, 1]. The discovery
288 of whole genome duplication in an invertebrate, and during horseshoe crabs' long and famously
conservative evolutionary history suggests that such events may have been more common than
290 previously assumed in metazoan evolution, and that while they may have provided raw material
for adaptive evolution in some cases, they are not evolutionary drivers.

Methods

292 Joint assembly and mapping (JAM) overview

294 Barcoded genomic DNA libraries were created, pooled, and sequenced in four lanes on the Illu-
mina HiSeq2000 platform for a mating pair of *L. polyphemus* and 34 offspring (Methods).

296 The JAM method proceeds through three major phases: 1. The frequencies of DNA sub-
sequences of fixed length k (k -mers) are profiled to characterize the quality, uniqueness, poly-
298 morphisms and repetition in genomic reads, using software we developed building on work from
the Atlas assembler[42]. Allelic pairs of k -mers representing alternate forms of single nucleotide
polymorphisms (SNPs) are identified and tracked through the subsequent steps. 2. Contigs are
300 assembled on a graph of unique k -mers and paired SNP k -mers sampled to reduce memory us-
age, then ordered and oriented using the Bambus scaffolder[26, 43]. Each multi-SNP scaffold is
302 treated as a single marker for the linkage mapping steps. 3. The paired SNP k -mers (SNPmers) in
each scaffold are combined with the read, mate-pair, and parent- or offspring-library associations
304 of their alleles for haplotype phasing and construction of a high density genetic linkage map.

Sampling and sequencing

306 Tissue samples were collected from the third walking leg of a monandrous pair of horseshoe crabs
nesting at high tide on the beach at Seahorse Key, an island along the west coast of north Florida,
308 on 27 March 2010. The eggs laid by this pair were collected 6 hr later when the tide had receded
and reared in plastic dishes as previously described[44]. Trilobite larvae hatched from the eggs 4
310 weeks later. Tissue samples and larvae were preserved in RNALater. Genomic DNA purification
and library construction were carried out using Qiagen DNAEasy, Illumina TruSeq and Nextera
312 kits, following manufacturers' protocols. Barcoded samples were pooled and sequenced on on the
Illumina HiSeq2000 platform.

314 *Limulus* larvae were processed as follows; each larva, suspended in 100 μ L of RNALater and
stored at -80 °C in a 1.5 mL Eppendorf tube, was thawed on ice, after which RNALater was re-
316 moved. DNA was extracted using the Qiagen DNAEasy kit per manufacturer's protocols. DNA
was quantified using picogreen DNA quantitation kit. To prepare TruSeq libraries, DNA was first
318 purified another time using zymo genomic DNA clean columns per manufacturer's protocols. Adult
L. polyphemus DNA was prepared as above, but using claw tissue rather than whole larvae. All
320 DNA extracts were tested by gel electrophoresis to ensure DNA was not degraded. TruSeq li-
braries were prepared at University of Georgia's Georgia Genomics Facility. 1-5 micrograms of
322 sample DNA was subjected to fragmentation using Covaris sonicator. Fragmented DNA was then

324 used for library construction using Illumina TruSeq library prep kits. Libraries were pooled together
326 in equimolar amounts (for 10 larvae) and used for sequencing. For samples 11-34, Library prep
328 was switched from TruSeq to Nextera kits. Nextera library preparation was performed according to
330 manufacturer's protocol. The Nextera library product was quantified by picogreen, and fragment
size distribution was checked by using Lonza flash gel, to ensure that fragment size distribution
was between 300-1000 bp. Sample libraries were pooled in equimolar concentrations and sent
for sequencing. Library pools were sequenced on the Illumina HiSeq2000 platform at Medical
College of Wisconsin Sequencing Service Core Facility.

***k*-mer decomposition**

332 We determine a lower bound on the *k*-mer size long enough for a given expectation of uniqueness
334 in a random genome. While increasing *k* reduces the rate of coincidentally repeated *k*-mers, it
336 also reduces the effective depth of coverage due to untrimmed errors and edge effects at read
338 ends — and increases the cases of multiple SNPs per *k*-mer locus, which are not tracked in our
current software implementation. We can approximately model a genome-scale string *G* of random
nucleotides as *G* samples taken with uniform probability from the space of all *k*-mers (of size $4^{k/2}$
for odd *k*-mers treating reverse-complements as same; slightly more for even *k*). The Poisson
distribution then gives the probability that a location in *G* has its own, unique *k*-mer (shared with
no other location) as

$$e^{-\lambda}, \text{ where } \lambda = G/(4k/2) = 2G/4k.$$

342 The probability of a location sharing its *kmer* is then $1 - e^{-\lambda}$; thus, to limit the maximum rate
344 *R* of *G*-locations sharing *k*-mers, we require $k \geq \lceil \log_4(-2G/\ln(1 - R)) \rceil$. For example, for a
mammalian-scale genome of approximately 3 billion bases, and *R* = 0.1%, we choose $k \geq 22$.
346 For *Limulus polyphemus*, the Animal Genome Size Database[25] reports an estimated haploid
genome size of 2.80 pg and, as each picogram represents almost a billion nucleotide base-pairs
of DNA, the mammalian-scale choice of *k* applies.[45, 19]

348 This lower bound ignores chemical and biological sequence biases, so selecting *k* for a real
350 genome project requires attention to error rates, repeats tandem and interspersed, and genome
size, all known vaguely, if at all, before sequencing. Studying the *k*-mer distributions after sequenc-
352 ing can clarify these genomic properties as we select *k* to maximize the net yield of candidate
k-mer tags, between errors and with at most one SNP location, in sequencing reads. We convert
Illumina/Solexa FASTQ format (paying attention to the different quality encodings of the software
354 versions) into FASTA format[46], masking (replacing with 'N') any base with Phred-scale[47] qual-
ity below 20, and soft-masking (representing in lower case) other bases with quality below 30.
356 For initial trimming experiments, we vary these quality thresholds as indicated below. We store
k-mers in hash tables with open addressing[48], supporting odd $k \leq 31$. We tally for each *kmer*
358 a bit vector for presence or absence in up to 64 libraries, and an overall count of occurrences in
all libraries (count limited to $64 - 2k$ bits) Where the *kmer* hash would be too large for available
360 memories, we sample the *kmers* using a hash-slicing factor *S* (must be prime). Representing each
kmer as an integer in $[0..4^k - 1]$, slice *s* consists of those *kmers* whose remainder on division by *S*
362 is *s*. We can tabulate one slice for a representative sample of $1/S$ *kmers* (for initial estimation of
depth of coverage and genome size) or, using *S* independent jobs, collect information for *kmers* in
364 all slices. Our hash tables store odd-length *kmers* so that reverse-complementary sequences can
be combined without the ambiguous orientation of palindromic sequences (e.g., ATCGAT).

366 After selecting *k* as described above and making a full tabulation of *kmer* counts and bit vec-
tors, we filter out *kmers* not expected to represent genomic sequence. *k*-mers were required to

368 have three copies in the total sequence set, with at least one copy in the initial run and one in the
370 second run. This was partly to filter out incomplete adapter sequences, which can be difficult to
trim but which were different in the two runs.

372 Extending methods developed for the Atlas assembler[42] to heterozygous sequences, Figure
374 1 gives a rough decomposition of the k -mer frequency distribution for 23-mers with quality \geq
20, minimizing the square of the residuals of k -mer counts on frequencies 3 through 70 while
376 not exceeding the observed counts. Four linked distributions model fractions of the genome as
monoallelic or biallelic: homozygous regions with $d = 38.9$ -fold coverage (dark blue), minor alleles
378 covered at $d/4$ (green), tied alleles at $d/2$ (red) and major alleles at $3d/4$ (purple). This fit is
robust enough to confirm the abundance of major-minor allele pairs (27 percent of k -loci, vs. 10
percent for tied alleles), with the broader peaks in the data than in the fitted curves consistent
with less uniform sampling (for example, varying coverage of parents and offspring). The Poisson
380 decomposition suggests a density of polymorphisms of 1.2% in major-minor allele pairs, based
on dividing the modeled number of such sequenced pairs by k (assuming most polymorphisms
382 are SNPs spaced at least k bases apart), by d (the estimated depth of sequencing) and by the
estimated genome size of 2.74 billion bases.

384 SNPmer identification

The filtered kmer counts, computed in parallel, are loaded into a hash table with additional fields
386 to track kmers that are uniquely within one mismatch of each other. Because this step analyzes
all (non-error) k -mers in one table, this requires a single large-memory processor (on the order of
388 32 GiB).

For each k -mer, we check all its $3k$ one-substitution neighbors. The k -mers are partitioned each
390 into one of three categories: *unique*: having no edit-neighbors within one substitution; *ambiguous*:
having either multiple one-substitution neighbors, or one neighbor that has multiple neighbors;
392 or *partnered*: uniquely pairable with exactly one other k -mer differing by one substitution, such
kmers also known from now on as SNPmers or SNPmer pairs. For each SNPmer, we save the
394 position of the substitution, a bitmask for the change (transition, complement, or non-complement
transversion), and whether the canonical form of the partner in the table has the same sense or is
396 reverse complemented with respect to this k -mer.

Only partnered and unique k -mers will be further tracked. While this limited method cannot
398 identify k -mers for genomic SNP and non-SNP locations with complete confidence, false pairing
or missed pairing should have limited effects on subsequent analysis. False pairing, due to co-
400 incidental similarities or repeats, will combine nodes of the k -mer graph (see below) and cause
possible misassembly: for our purposes, noise in the scaffolding, haplotype phasing, and linkage
402 analysis. Missed pairing can happen from indel polymorphisms, SNPs separated by fewer than
 $k - 1$ positions, failure to sequence minor alleles, or ambiguity due to too many similar k -mers.
404 Ambiguously non-unique k -mers will be skipped over (reducing connectivity of the k -mer graph if
there are too many in a row). While allelic k -mers misidentified as unique will cause more forks
406 in the k -mer graph, those from major-alleles will still be chained together with flanking unique se-
quence, provided that major allele k -mers have at least twice the frequency as those for the minor
408 allele.

Table 2 shows the totals and percentages of the different kmer categories, counting each
410 SNPmer pair as one kmer. SNPmer pairs account for 16.3 percent of the putative genomically
unique 23mer markers; dividing by 23 gives us the fraction of bases in those markers that are
412 putative SNPs: 0.71 percent.

Table 2: K-mer categories, counting a SNPmer pair as one kmer

<i>k</i> -mer type	# Distinct	Percentage
no partner/unique	946,431,901	55.48%
partnered/SNPmer	184,756,149	10.83%
ambiguous	574,557,296	33.68%
TOTAL	1,705,745,346	

Subset *k*-mer selection

414 To reduce the memory requirements of our *k*-mer assembly graph, we select a roughly one-tenth
 416 subset of the *k*-mers .

416 In the case of a true SNP at least *k*-1 bases from other SNPs and gaps in error-free coverage
 418 of either allele, there will be *k* covering SNPmer pairs (provided that covering *k*-mers are also
 418 uniquely pairable). By taking only SNPmer pairs with the substitution in particular positions, we
 420 can reduce the size of the graph and its redundancy. Analyzing the distribution of edit position for
 420 all the SNPmer pairs, we observe an enrichment for edits near the ends due to sequencing errors.
 422 By selecting positions 3, 12 and 21 of 23-base SNPmers, we avoid the most problematic positions
 422 and reduce this portion of *k*-mer nodes by a factor of 7.67.

424 Unlike for SNPmers, there are no canonical positions that identify the unique, unpaired *k*-mers
 424 . Several mechanisms have been proposed for sampling *k*-mers in a representative way[49, 50].
 426 We use the more pseudo-random hash-slicing rule, already discussed above, to sample a single
 426 slice of *k*-mers those whose integer encodings are congruent to a particular slice number *s*,
 428 modulo *S* (the hash slicing factor). We have found that on the finished human genome (results not
 428 shown), hash slicing is effectively a Poisson sampling, with sampled *k*-mers spaced according to
 an exponential distribution.

430 A caveat in applying hash slicing is that taking the remainder modulo a prime is not very
 430 pseudo-random for Mersenne primes (equal to 2^{p-1} for some *p*), when *k*-mers are represented in
 432 base-4 encoding[48]. We therefore pick a slicing factor of 11, the smallest non-Mersenne prime
 432 greater than our SNPmer sampling factor.

434 The resulting *k*-mer subset has 86.0 million unpaired *k*-mers and 24.0 million SNPmer pairs,
 each reduced as predicted, for a total factor of 9.8 reduction in *k*-mer nodes for the next step.

436 Contigging and scaffolding

436 Each of the sampled unique *k*-mers and SNPmer pairs is a node in the *k*-mer graph. Nodes
 438 are connected when the corresponding *k*-mers appear consecutively in at least one read of the
 438 input (any intervening *k*-mers having been skipped due to sampling or ambiguity). The relative
 440 orientation, distance and number of supporting reads of the *k*-mers is stored in the edge. When
 440 conflicting distance or relative orientation is observed among different reads for the same pair of
 442 *k*-mer nodes, all edges from both nodes in the corresponding direction are ignored in contigging.

444 Robust edges for one direction from a node are defined as those supported by a supermajority
 444 of the reads containing the *k*-mer: the number of supporting reads is greater than or equal to both
 446 (1) two plus the sum of the read counts for all other edges in that direction and (2) twice the read
 446 count of the next-most supported edge in the same direction. By this construction, a node has at
 most one robust edge in each direction.

448 A mutually robust edge is defined as one that is robust going in both directions between the
two nodes it connects.

450 Contigs are the connected components of the subgraph consisting of mutually robust edges.
Singleton and circular contigs are reported for diagnostic purposes, but ignored in subsequent
452 analysis. Each retained “ k -mer contig” of Table 1 therefore represents a chain of nodes for
SNPmers and unique k -mers not shared with other contigs.

454 After assembly of k -mer contigs, we connect them in longer structures using the Bambus
scaffolder[26]. This requires mapping templates (read pairs) to contigs, based on shared k -mer
456 content, and dividing the resulting graph of contigs linked by templates into batches small enough
for Bambus to process.

458 Contigs are chains of k -mer nodes (unique or SNPmers). Since each node can appear only
once in the contigs, contigs can be represented with a variant of the k -mer hash. This allows
460 efficient tabulation of template-to-contig overlaps in a single pass through the read cdata. Each
overlap is detected by the number of shared k -mers on a consistent diagonal (*i.e.* relative se-
462 quence offset) and their span on read and contig. Templates that overlap multiple contigs can be
used to order and orient those contigs.

464 We present templates linking contigs to Bambus using AMOS format[43] for the reads (tem-
plate ends) mapped to each contig. Reads are included only for the contig with which it shares the
466 most k -mers, if the span of those $\{k\text{-mers}\}$ is $\geq k$ and the other read-end of the template similarly
qualifies in a different contig. Bambus then infers links between contigs by matching template
468 identifiers shared by reads in different “linkable contigs”.

To generate independent AMOS files for each Bambus run, the large graph of template links
470 is partitioned into connected components. These components are grouped into batches for a rea-
sonably load-balanced parallel computation with no template links between batches. The results
472 are summarized as “initial scaffolds” in Table 1.

474 Consensus sequence representations for $\{k\text{-mer}\}$ contigs and scaffolds were generated in two
phases. In the first phase, sequence spanned by selected SNPmers and subset $\{k\text{-mers}\}$ (see
476 sections and above) are joined together, separated by a number of Ns corresponding to the
number of bases not spanned by $\{k\text{-mers}\}$ in the subset. In the second phase, a single pass is
478 made through the read data set, and stretches of Ns that are spanned by single reads are replaced
by the sequence of the read.

SNP phase and genotype inference

480 Each scaffold of the k -mer assembly constitutes a candidate marker for mapping. While the depth
of sequence coverage on each member of the mapping panel is too low (about 1X) to directly
482 infer the genotype of individual members of the mapping pannel at individual SNPs, the tight link-
age between SNPs within markers means that learning a sample’s genotype at any one reveals
484 it at the others, effectively amplifying the sequence coverage by a factor proportional to the num-
ber of SNPs within the marker. This is the same principle exploited in genotype by sequencing
486 (GBS) approaches to genetic mapping in the presence of reference genomes, for example in re-
combinant inbred lines of reference rice strains[16], and in crosses between *Drosophila* species
488 with sequenced genomes[17]. We use the same principle to genotype offspring in the context of
a cross between two outbred individuals, simultaneously inferring the phases of the SNPs (*i.e.*
490 which bases appears on each of the four parental chromosomes in the cross).

492 While the data will be insufficient to infer genotypes at many markers, all those where confident
inferences can be made can be used to build the linkage map.

494 For the purposes of genotype inference, a marker is treated as a collection of m SNPs (indexed
 in the following by $i \in \{1, 2, \dots, m\}$), that have been inferred to be closely linked on the genome via
 the k -mer assembly step. If the four parental chromosomes are labeled a, b in one parent and c, d
 496 in the other, then the genotyping problem is to infer which of the four possible segregation states
 or genotypes ac, ad, bc, bd describes each sample at each marker locus. We index samples with j ,
 498 and denote a sample genotype by g_j .

We assume that markers are very small compared to a chromosome, and ignore the possibility
 500 of a recombination event within individual markers. The data used for inference of the offspring
 genotypes consist of the number of reads from each barcoded sample j showing each of the four
 502 possible DNA bases b at each variable SNP position i , which we denote n_{ij}^b .

If the phase ϕ_i of SNP i were known, *i.e.* which base is present in each of the four parental
 504 chromosomes, then a choice of genotype g_j implies a specific homozygous or heterozygous state
 $s_{ij} \in S = \{AA, CC, TT, GG, AC, AT, AG, CT, CG, TG\}$ for SNP i in sample j . For a given phase
 506 and genotype, the likelihood function for a given SNP position in a given sample is given by either
 a binomial (for homozygous states) or trinomial probability mass function of the read counts, base-
 508 calling error rate ϵ , and the site genotype s_{ij} :

$$\mathbb{L}(\phi_i, g_j) = p(n_{ij}^b | \phi_i, g_j) = P_m(n_{ij}^b, s_{ij}, \epsilon) = \begin{cases} \binom{n}{m} \epsilon^m (1 - \epsilon)^{n-m}, & \text{if } s_{ij} \text{ homozygous} \\ \frac{n!}{k!l!m!} \epsilon^m \left(\frac{1-\epsilon}{2}\right)^{k+l}, & \text{if } s_{ij} \text{ heterozygous} \end{cases}$$

where n is the total number of reads at SNP i ; m is the number of observations of bases not
 510 in s_{ij} (*i.e.* mismatches); k and l are the counts for each of the two bases of s_{ij} for heterozygous
 sites, and $\epsilon = 2\epsilon/3$.

512 Likelihood maximization

Searching for an optimal choice of SNP phases ϕ_i and sample genotypes g_j is made difficult by
 514 the exponential size of the search space: for segregating bi-allelic SNP sites there are 14 possible
 phases to consider at each SNP site, so for a mapping panel of only 20 siblings and a marker
 516 containing only 10 SNPs, there are $4^{20} \times 14^{10} > 3 \times 10^{23}$ combinations to consider. In simulation
 tests, we found that a variant of expectation maximization (EM), an iterative likelihood maximization
 518 method can accurately infer a large proportion of marker genotypes.

To initialize the iteration, the parental samples and a randomly selected offspring are, without
 520 loss of generality, assigned genotypes (a, b) , (c, d) and (a, c) . At each step, we calculate the condi-
 tional probability distributions over the possible SNP phases $p(\phi_i)$ given the genotype assignments
 522 according to:

$$p^{(t)}(\phi_i) = p(\phi_i | \mathbf{g}^{(t)}) = \prod_{\sigma \in S} p(n_{i\sigma}^b | \phi_i, \mathbf{g}^{(t)}) / \left(\sum_k \prod_{\tau \in S} p(n_{k\tau}^b | \phi_k, \mathbf{g}^{(t)}) \right)$$

where we have labeled the chosen values for the genotypes g_j at iteration t collectively by $\mathbf{g}^{(t)}$.
 524 $n_{i\sigma}^b$ is the combined total number of observations of base b at polymorphic SNP i for all samples
 included at iteration step t which have genotype $s(\phi_i, g_j) = \sigma$.

On each iteration until all samples have been included, a randomly selected sample is added to
 526 the set after calculating $p^{(t)}(\phi_i)$. Then the next set of genotype assignments $\mathbf{g}^{(t+1)}$ are determined
 528 by choosing those that maximize the expected value of the log likelihood:

$$\mathbb{E}_{\phi|n,g_j}[\log L(g_j; n, \phi)] = \sum_i p(\phi_i) \log p(n_{ij}^b | g_j, \phi_i)$$

These steps are repeated until genotypes are being selected for all samples, and the expected log likelihood stops increasing. At the end of the iteration, the likelihood-maximizing genotypes are reported, along with the log likelihood difference between the best and second best choice of genotype for each sample, which provides an indicator of the confidence in genotype call. To gauge convergence, this procedure is repeated 5 times for each marker, with different random choices of initial conditions. Markers which do not identify the same ML genotype multiple times in independent runs are not included among the high confidence genotype calls.

Error model calibration

The sequence of 14 *Ciona intestinalis* autosomes were downloaded from Ensembl (www.ensembl.org). These 14 chromosomes were used as the template in our genome simulation. Based on their sequence length, We used a markovian coalescent simulator `macs` [51] to generate four haploid samples drawn from a population under neutral Wright-Fisher model with population mutation rate of 0.012 and population recombination rate of 0.0085. Using the *C. intestinalis* genome as the reference sequence, two diploid parental genomes were constructed based on the `macs` output with realistic SNP and Indel models inferred by several previous studies on the *Ciona* genome[52–54]. We wrote a `perl` script to simulate the genomes of offspring generated by the cross of the two simulated parents. The software package `dwgsim`[55] was used to generate Illumina paired-end reads based on our simulated genomes of both parents and offsprings, with the coverage of 20X and 5X respectively.

To estimate the frequency of incorrect genotype calls as a function of the log likelihood difference between the called and alternative genotype, including contributions from uncertainty in SNP-mer identification, assembly, and sampling noise, we carried out a simulation of the k -mer assembly and genotype inference protocols. Among high-confidence genotype calls, the observed error frequency was a function of call confidence score was well-fit by a sum of two stretched exponential functions, allowing assignment of error probabilities to individual genotype calls.

Linkage group construction

We use the linkage p-value p_{ab} between pairs of map bins a and b defined as the minimum over the four possible relabelings r of the maternal and paternal chromosomes of the Binomial p-value for the number of matching genotypes:

$$p_{ab} = \min_r \left[1 - \sum_i^{m_r-1} \binom{n}{i} \frac{1}{2^n} \right]$$

where n is the total number of sample genotype calls (68 in the present case, or 34 in each parent) and m_r is the number of matching genotypes under relabeling r .

We identified map bins with segregation patterns indicating either inconsistent placement in the maternal and paternal maps or genotyping error with a double threshold procedure as follows:

1. Map bins were partitioned into linkage groups by single linkage clustering at a threshold of $p_{ab} < p_1$.

564 2. Within each partition, map bins which formed articulation points[i.e. nodes which, if removed,
566 would cause the linkage group to fall apart into two disconnected subgraphs; 56] in the graph
of $p_{ab} < p_2$, where $p_2 > p_1$.

This procedure identifies map bins which alone account for the merging of what would other-
568 wise be two distinct partitions. We used the following pairs of thresholds p_1, p_2 to identify a total
of 20 map bins for exclusion from the map: $10^{-7}, 10^{-6}$; $10^{-8}, 10^{-7}$; $10^{-9}, 10^{-8}$. The remaining
570 markers form locally consistent linkage groups in which all linkages defined at threshold p_1 are
corroborated by multiple linkages at p_2 , for the above values of p_1 and p_2 .

572 **Marker ordering**

Markers were ordered within each linkage group using the following protocol. Within each link-
574 age group a consistent labeling of the four parental chromosomes was achieved by constructing
a graph G in which nodes correspond to map bins and edges are weighted by linkage p-value p_{ab}
576 (as defined above). The local chromosome labels are updated at each map bin as it is reached in
a traversal of the minimum spanning tree of G to the labeling r that maximizes p_{ab} along the inci-
578 dent of G used in the traversal. Markers within each linkage group were clustered by hierarchical
clustering (marker-marker distance metric: cosine of the angle between the vectors of recombi-
580 nation distances to the other map bins; distance updating method: average linkage) into a binary
tree data structure with leaves representing map bins. A node in the right subtree of the root node
582 was rotated, interchanging its left and right subtrees if its left subtree was not already closer (in
average recombination distance) to the markers of the left subtree of the global root; and similarly
584 for nodes in the left subtree of the root. An in-order traversal of the tree generates an ordering of
the markers. Finally three reversals of the order of markers in segments of the map were added
586 based on visual inspection of the recombination distance matrix. In the final marker ordering, 51%
of adjacent map bin pairs are separated by a single recombination event in the cross, and 94%
588 are separated by three or fewer recombinants in each parent.

Placement of markers on the map

590 To anchor additional markers to the map, we computed the p_{ab} (see above) between marker a to
be placed on the map and each map bin b . Marker a is anchored to the map at the position of the
592 bin b which minimizes p_{ab} if $p_{ab} < 10^{-6}$.

SNP density estimation

594 Illumina reads were mapped to the assembled scaffold sequences with `stampy`[57] using default
settings. For a sample of 9,228 scaffolds with lengths ranging from 5.0-5.5 kb, sequence variants
596 were called with `SAMtools`[58] using a variant quality score threshold of 50, and ignoring indel
positions.

598 A SNP density of 0.76 % in four haplotypes which corresponds to a predicted rate of pairwise
sequence differences per site of $\theta = 0.0042$ under the finite sites model of mutation and the neutral
600 coalescent model of the relationships among sampled alleles[59].

Estimation of local recombination rate

602 To estimate the local recombination rate for each map bin, we computed the linear regression of
map distance in number of markers on physical distance using up to 10 neighboring map bins
604 in each direction along the map (or fewer for bins within 10 map bins of the end of the linkage
group). Map distance was calculated from recombination fraction using Haldane's map distance
606 $-\frac{1}{2}\log(1 - 2r)$ [60].

Ancestral linkage group conservation

608 To compare the genome organization in *L. polyphemus* to the ancestral metazoan ALGs, we used
the reciprocal best blast hit (RBH) orthology criterion in an alignment of the *Ixodes scapularis*
610 predicted proteins[32] to the consensus sequences for the marker scaffolds. *L. polyphemus* scaf-
folds with RBH of e-value $\leq 10^{-6}$ were assigned to the same ancestral bilaterian gene orthology
612 group as their *I. scapularis* ortholog, and thereby with human genes. Regions of the map were
tested for enrichment in genes from particular ancestral linkage groups with Fisher's Exact Test,
614 and breakpoints in ancestral linkage group composition were identified using a hidden Markov
model, as previously described[6, 7].

Homeobox gene modeling

616 We identified 155 marker scaffolds with a tblastx alignment of e-value $< 10^{-6}$ to a set of che-
licerate homeobox gene sequences downloaded from Genbank using the NCBI online query in-
618 terface (genbank accessions AF071402.1, AF071403.1, AF071405.1, AF071406.1, AF071407.1,
AF085352.1, AF151986.1, AF151987.1, AF151988.1, AF151989.1, AF151990.1, AF151991.1,
620 AF151992.1, AF151993.1, AF151994.1, AF151995.1, AF151996.1, AF151997.1, AF151998.1,
AF151999.1, AF152000.1, AF237818.1, AJ005643.1, AJ007431.1, AJ007432.1, AJ007433.1, AJ007434.1,
622 AJ007435.1, AJ007436.1, AJ007437.1, AM419029.1, AM419030.1, AM419031.1, AM419032.1,
DQ315728.1, DQ315729.1, DQ315730.1, DQ315731.1, DQ315732.1, DQ315733.1, DQ315734.1,
624 DQ315735.1, DQ315736.1, DQ315737.1, DQ315738.1, DQ315739.1, DQ315740.1, DQ315741.1,
DQ315742.1, DQ315743.1, DQ315744.1, EU870887.1, EU870888.1, EU870889.1, HE608680.1,
626 HE608681.1, HE608682.1, HE805493.1, HE805494.1, HE805495.1, HE805496.1, HE805497.1,
HE805498.1, HE805499.1, HE805500.1, HE805501.1, HE805502.1, S70005.1, S70006.1, S70008.1,
628 and S70010.1). The reads of each marker (those with best `stampy`[57] alignment to the scaffold)
were reassembled with `PHRAP`[61], with default parameters. The resulting contigs were aligned to a
630 collection of homeobox-containing protein sequences (genbank accessions NP 001034497.1, NP
001034510.1, AAL71874.1, NP 001034505.1, NP 001036813.1, CAA66399.1, NP 001107762.1,
632 NP 001107807.1, EEZ99256.1, NP 001034519.1, NP 476954.1, NP 032840.1, NP 031699.2,
AAI37770.1, EEN68949.1, NP 523700.2, NP 001034511.2, AAK16421.1, and AAK16422.1) with
634 `exonerate`[62] in protein-to-genome mode. For each contig, the amino acid sequence predicted by
the highest-scoring `exonerate` alignment was used in subsequent phylogenetic analysis, resulting
636 in 104 putative homeobox-containing markers ranging in length from 18 to 147 amino acids.

Phylogenetic analysis of homeobox genes

638 A multiple sequence alignment of the predicted homeobox sequences combined with a collec-
640 tion of representative sequences from various classes of homeobox genes was constructed with
`muscle3.8.31`[63] using default settings. The resulting alignment was trimmed to a 63 amino acid

642 segment spanning the conserved homeodomain, and sequences with more than 50% gaps were
644 removed, leaving 93 predicted *L. polyphemus* homeobox genes in the analysis. Bayesian phyloge-
646 netic analysis was carried out on the resulting 178 taxon, 63 amino acid character matrix (Supple-
648 mentary File HomboboxTable.html) using MrBayes v3.2.1[64] using a mixed model of amino acid
650 substitutions, gamma-distributed rate variation among sites with fixed shape parameter $\alpha = 1.0$,
652 alignment gaps treated as missing data, 2,000,000 Monte Carlo steps, two independent runs with
654 four Monte Carlo chains, and the initial 25% of sampled trees were discarded as “burn-in”. Monte
Carlo appeared to reach convergence, with an average standard deviation of the split frequencies
of 0.022. The majority-rule consensus of the sampled trees is shown in Figures 6 and 7, and
well-supported gene clades (posterior probability greater than 0.95) were used to group the pre-
dicted *L. polyphemus* genes into classes. The table in Supplementary File HomboboxTable.html
lists the reassembled marker contigs, their inferred hox gene class, and maximum likelihood map
positions. Predicted genes were anchored to the map as described above.

Genomic distribution of paralogs

656 We identified 2716 pairs of *Limulus* markers that can both be placed on the map and have their
658 best translated alignment to the same *I. scapularis* gene. (*I. scapularis* genes with more than five
660 best-hit markers were excluded from seeding such pairs.) To estimate the synonymous sequence
662 divergence between pairs of candidate *L. polyphemus* paralogous gene pairs and *L. polyphemus*
664 genes and their *T. tridentatus* orthologs, we constructed codon alignments of predicted coding
sequence for estimation of synonymous sequence divergence. Conserved clusters of paralogs
were identified using a variant of the “max-gap” criterion[3] in which two genes are placed in the
same cluster if they and their paralogs lie within threshold distance. In the analysis presented
here, the distance threshold used was 500 markers.

K_a and K_s estimation for paralogs and *T. tridentatus* orthologs

666 Figure 8 shows the distribution across the map of pairs of candidate paralogs.

668 To estimate the synonymous sequence divergence between pairs of candidate *L. polyphemus* paralogous gene pairs, and between *L. polyphemus* genes and their *T. tridentatus* orthologs, we followed the following protocol.

- 670 1. Reassemble reads from each marker with PHRAP[61], and create a predicted coding sequence using exonerate, as described for the annotation of homeobox gene models (see 672 above).
- 674 2. Combine the exonerate alignments of codons to amino acids to create an alignment of codons for either a pair of *L. polyphemus* sequences, or for a *L. polyphemus* - *T. tridentatus* sequence pair.
- 676 3. Use the method of Yang and Nielsen[65] to estimate the synonymous and non-synonymous substitution rates K_a and K_s , as implemented in the KaKsCalculator package[66].
- 678 4. Discard estimates based on fewer than 30 sites (30 synonymous sites for estimates of K_s , non-synonymous sites for K_a).

680 GenBank accessions for *Tachypleus tridentatus* mRNA clones: JQ966943, AB353281, AB353280, HM156111, HQ221882, HQ221883, HQ221881, HQ386702, HM852953, TATTPP, TATPROCLOT, 682 FN582225, FN582226, AF467804, AF227150, GQ260127, AF264067, AF264068, AB353279, AB005542, TATLICI, TATTGL, TATCFGB, TATLFC1, TATLFC2, AB201713, TATCFGA, TATLICI2, 684 CS423581, CS423579, AB028144, AB201778, AB201776, AB201774, AB201772, AB201770, AB201768, AB201766, AB201779, AB201777, AB201775, AB201773, AB201771, AB201769, 686 AB201767, AB201765, AB105059, AB002814, AX763473, TATCFBP, AB076186, AB076185, X04192, TATHCLL, AB037394, AB019116, AB019114, AB019112, AB019110, AB019108, AB019106, AB019104, 688 AB019102, AB019100, AB019098, AB019096, AB019117, AB019115, AB019113, AB019111, AB019109, AB019107, AB019105, AB019103, AB019101, AB019099, AB019097, AB023783, 690 AB024738, AB024739, AB024737, AB017484, D87214, D85756, D85341.

692 Figure 9 shows the distributions of K_a and K_s for paralogs and *T. tridentatus* orthologs. To estimate the number and age of peaks in the un-saturated range[33] of the K_s distribution (and of putative WGD events), we fit a series of univariate normal mixture models, with 1, 2, 3, and 4 694 components to the paralog K_s distribution in the range $0 < K_s < 2.5$ and selected the best model on the basis of Bayesian Information Criterion (Table 3). The best model had two components, 696 with means at 0.7 and 1.45 substitutions per site. The position of the peak at lowest K_s was not sensitive to the addition of more mixture components. Figure 10 shows a comparison of the distribution and the components of the best-fitting model. Gaussian mixture models were 698 estimated in R with `mixtools`[67].

700 Data Access

702 The raw sequencing reads are currently being submitted through the NCBI SRA and are accessible via NCBI BioProject accession PRJNA187356.

Table 3: Mixture model fits to K_s distribution. N is the number of mixture components, k the number model parameters, ln(L) the log likelihood of the data under the best fit model, BIC the Bayesian information criterion, AIC the Akaike information criterion.

N	k	ln(L)	BIC	AIC	mixture components
1	2	-273.93	559.74	551.87	1.32 ± 0.50
2	5	-259.32	548.31	528.64	0.70 ± 0.14 ; 1.45 ± 0.45
3	8	-253.36	554.19	522.71	0.71 ± 0.17 ; 1.34 ± 0.29 ; 2.09 ± 0.19
4	11	-251.41	568.11	524.82	0.74 ± 0.18 ; 1.34 ± 0.20 ; 1.70 ± 0.04 ; 2.02 ± 0.22

Acknowledgements

704 This research was supported by the National Science Foundation (EF-0850294 and IOB 06-
 41750), the Beckman Young Investigator Program, the University of Florida Division of Sponsored
 706 Research, the Department of Biology, and the UF Marine Laboratory at Seahorse Key.

Author contributions

708 NHP conceived and led the project. All authors wrote the paper. PH, NHP and J-XY wrote soft-
 ware. NHP, PH, J-XY and CWN carried out sequence analysis. JB collected and raised samples.
 710 CWN extracted genomic DNA and created the libraries for sequencing.

Discosure Declaration

712 The authors declare that they have no conflicts of interest.

Figures

714

References

- 716 [1] Ohno S (1970) Evolution by gene duplication. Springer-Verlag.
- [2] Wolfe KH, Shields DC (1997) Molecular evidence for an ancient duplication of the entire yeast
 718 genome. *Nature* 387: 708–713.
- [3] McLysaght A, Hokamp K, Wolfe KH (2002) Extensive genomic duplication during early chor-
 720 date evolution. *Nature Genetics* 31: 200–204.
- [4] Simillion C, Vandepoele K, Montagu MCEV, Zabeau M, Peer YVd (2002) The hidden dupli-
 722 cation past of arabidopsis thaliana. *Proceedings of the National Academy of Sciences* 99:
 13627–13632.

- 724 [5] Aury JM, Jaillon O, Duret L, Noel B, Jubin C, et al. (2006) Global trends of whole-genome
duplications revealed by the ciliate paramecium tetraurelia. *Nature* 444: 171–178.
- 726 [6] Putnam NH, Srivastava M, Hellsten U, Dirks B, Chapman J, et al. (2007) Sea anemone
728 genome reveals ancestral eumetazoan gene repertoire and genomic organization. *Science*
317: 86–94.
- [7] Putnam NH, Butts T, Ferrier DEK, Furlong RF, Hellsten U, et al. (2008) The amphioxus
730 genome and the evolution of the chordate karyotype. *Nature* 453: 1064–1071.
- [8] Srivastava M, Begovic E, Chapman J, Putnam NH, Hellsten U, et al. (2008) The trichoplax
732 genome and the nature of placozoans. *Nature* 454: 955–960.
- [9] Srivastava M, Simakov O, Chapman J, Fahey B, Gauthier MEA, et al. (2010) The amphime-
734 don queenslandica genome and the evolution of animal complexity. *Nature* 466: 720–726.
- [10] Simakov O, Marletaz F, Cho SJ, Edsinger-Gonzales E, Havlak P, et al. (2012) Insights into
736 bilaterian evolution from three spiralian genomes. *Nature* .
- [11] Lv J, Havlak P, Putnam N (2011) Constraints on genes shape long-term conservation of
738 macro-synteny in metazoan genomes. *BMC Bioinformatics* 12: S11.
- [12] Earl D, Bradnam K, John JS, Darling A, Lin D, et al. (2011) Assemblathon 1: A competitive
740 assessment of de novo short read assembly methods. *Genome Research* 21: 2224–2241.
- [13] Davey JW, Hohenlohe PA, Etter PD, Boone JQ, Catchen JM, et al. (2011) Genome-wide
742 genetic marker discovery and genotyping using next-generation sequencing. *Nature Reviews*
Genetics 12: 499–510.
- [14] Altshuler D, Pollara VJ, Cowles CR, Van Etten WJ, Baldwin J, et al. (2000) An SNP map of
744 the human genome generated by reduced representation shotgun sequencing. *Nature* 407:
746 513–516.
- [15] Baird NA, Etter PD, Atwood TS, Currey MC, Shiver AL, et al. (2008) Rapid SNP discovery
748 and genetic mapping using sequenced RAD markers. *PLoS ONE* 3: e3376.
- [16] Huang X, Feng Q, Qian Q, Zhao Q, Wang L, et al. (2009) High-throughput genotyping by
750 whole-genome resequencing. *Genome Research* 19: 1068–1076.
- [17] Andolfatto P, Davison D, Erezyilmaz D, Hu TT, Mast J, et al. (2011) Multiplexed shotgun geno-
752 typing for rapid and efficient genetic mapping. *Genome Research* 21: 610–617.
- [18] Chapman JA, Ho I, Sunkara S, Luo S, Schroth GP, et al. (2011) Meraculous: De novo genome
754 assembly with short paired-end reads. *PLoS ONE* 6: e23501.
- [19] Butler J, MacCallum I, Kleber M, Shlyakhter IA, Belmonte MK, et al. (2008) ALLPATHS: de
756 novo assembly of whole-genome shotgun microreads. *Genome Research* 18: 810–820.
- [20] Gnerre S, MacCallum I, Przybylski D, Ribeiro FJ, Burton JN, et al. (2011) High-quality draft
758 assemblies of mammalian genomes from massively parallel sequence data. *Proceedings of*
the National Academy of Sciences 108: 1513–1518.

- 760 [21] Rudkin DM, Young GA (2009) Horseshoe crabs – an ancient ancestry revealed. In: Tanacredi
762 JT, Botton ML, Smith D, editors, *Biology and Conservation of Horseshoe Crabs*, Springer US.
pp. 25–44. URL <http://www.springerlink.com/content/t231746300u44q55/abstract/>.
- [22] Fisher DC (1984) The xiphosurida: archetypes of bradytely? In: Eldrege N, Stanley SM,
764 editors, *Living Fossils*, Springer Verlag. pp. 196–213.
- [23] Berkson J, Shuster CN Jr (1999) The horseshoe crab: The battle for a true multiple-use
766 resource. *Fisheries* 24: 6–10.
- [24] Shuster CN Jr, Barlow RB, Brockmann HJ, editors (2003) *The American Horseshoe Crab*.
768 Cambridge, MA: Harvard University Press.
- [25] Gregory TR (2012). *Animal genome size database*. URL AnimalGenomeSizeDatabase.
- 770 [26] Pop M, Kosack DS, Salzberg SL (2004) Hierarchical scaffolding with bambus. *Genome Re-*
search 14: 149–159.
- 772 [27] van Os H, Andrzejewski S, Bakker E, Barrena I, Bryan GJ, et al. (2006) Construction of a
10,000-marker ultradense genetic recombination map of potato: Providing a framework for
774 accelerated gene isolation and a genomewide physical map. *Genetics* 173: 1075–1087.
- [28] Iwasaki Y, Iwami T, Sekiguchi K (1988) Karyology. In: Sekiguchi K, editor, *Biology of Horse-*
776 *shoe Crabs*, Tokyo: Science House Co. pp. 309–314.
- [29] Cartwright RA, Hussin J, Keebler JEM, Stone EA, Awadalla P (2012) A family-based proba-
778 bilistic method for capturing de novo mutations from high-throughput short-read sequencing
data. *Statistical applications in genetics and molecular biology* 11.
- 780 [30] Bird AP (1980) DNA methylation and the frequency of CpG in animal DNA. *Nucleic Acids*
Research 8: 1499–1504.
- 782 [31] Lynch M (2006) The origins of eukaryotic gene structure. *Molecular Biology and Evolution*
23: 450–468.
- 784 [32] VectorBase (2008). *Ixodes scapularis* annotation, IscaW1. URL <http://www.vectorbase.org>.
- 786 [33] Vanneste K, Van de Peer Y, Maere S (2013) Inference of genome duplications from age
distributions revisited. *Molecular biology and evolution* 30: 177–190.
- 788 [34] Obst M, Faurby S, Bussarawit S, Funch P (2012) Molecular phylogeny of extant horseshoe
crabs (xiphosura, limulidae) indicates paleogene diversification of asian species. *Molecular*
790 *Phylogenetics and Evolution* 62: 21–26.
- [35] Begun DJ, Aquadro CF (1992) Levels of naturally occurring DNA polymorphism corre-
792 late with recombination rates in *d. melanogaster*. , Published online: 09 April 1992; |
doi:101038/356519a0 356: 519–520.
- 794 [36] Cutter AD, Payseur BA (2003) Selection at linked sites in the partial selfer *caenorhabditis*
elegans. *Molecular Biology and Evolution* 20: 665–673.
- 796 [37] Nachman MW (2001) Single nucleotide polymorphisms and recombination rate in humans.
Trends in Genetics 17: 481–485.

- 798 [38] Stephan W, Langley CH (1998) DNA polymorphism in lycopersicon and crossing-over per
physical length. *Genetics* 150: 1585–1593.
- 800 [39] Roselius K, Stephan W, Städler T (2005) The relationship of nucleotide polymorphism, re-
combination rate and selection in wild tomato species. *Genetics* 171: 753–763.
- 802 [40] Hellmann I, Ebersberger I, Ptak SE, Pääbo S, Przeworski M (2003) A neutral explanation
for the correlation of diversity with recombination rates in humans. *The American Journal of*
804 *Human Genetics* 72: 1527–1535.
- [41] Andolfatto P, Przeworski M (2001) Regions of lower crossing over harbor more rare variants
806 in african populations of drosophila melanogaster. *Genetics* 158: 657–665.
- [42] Havlak P, Chen R, Durbin KJ, Egan A, Ren Y, et al. (2004) The atlas genome assembly
808 system. *Genome Research* 14: 721–732.
- [43] Treangen TJ, Sommer DD, Angly FE, Koren S, Pop M (2011) Next generation sequence as-
810 sembly with AMOS. *Current protocols in bioinformatics / editorial board, Andreas D Baxevanis*
[et al] CHAPTER: Unit11.8.
- 812 [44] Johnson SL, Brockmann HJ (2010) Costs of multiple mates: an experimental study in horse-
shoe crabs. *Animal Behaviour* 80: 773–782.
- 814 [45] Mullikin JC, Ning Z (2003) The phusion assembler. *Genome Research* 13: 81–90.
- [46] Cock PJA, Fields CJ, Goto N, Heuer ML, Rice PM (2010) The sanger FASTQ file format
816 for sequences with quality scores, and the Solexa/Illumina FASTQ variants. *Nucleic Acids*
Research 38: 1767–1771.
- 818 [47] Ewing B, Green P (1998) Base-calling of automated sequencer traces UsingPhred. II. error
probabilities. *Genome Research* 8: 186–194.
- 820 [48] Knuth DE (1973) Searching and Sorting, volume 3 of *The Art of Computer Programming*.
Reading, MA: Addison-Wesley.
- 822 [49] Roberts M, Hayes W, Hunt BR, Mount SM, Yorke JA (2004) Reducing storage requirements
for biological sequence comparison. *Bioinformatics* 20: 3363–3369.
- 824 [50] Ye C, Ma Z, Cannon C, Pop M, Yu D (2012) Exploiting sparseness in de novo genome as-
sembly. *BMC Bioinformatics* 13: S1.
- 826 [51] Chen GK, Marjoram P, Wall JD (2009) Fast and flexible simulation of DNA sequence data.
Genome Research 19: 136–142.
- 828 [52] Dehal P, Satou Y, Campbell RK, Chapman J, Degnan B, et al. (2002) The draft genome of
ciona intestinalis: Insights into chordate and vertebrate origins. *Science* 298: 2157–2167.
- 830 [53] Haubold B, Pfaffelhuber P, Lynch M (2010) mlRho – a program for estimating the popula-
tion mutation and recombination rates from shotgun-sequenced diploid genomes. *Molecular*
832 *Ecology* 19: 277–284.
- [54] Small KS, Brudno M, Hill MM, Sidow A (2007) Extreme genomic variation in a natural popu-
834 lation. *Proceedings of the National Academy of Sciences* 104: 5698–5703.

- [55] Homer N (2012). dwgsim. URL <http://sourceforge.net/apps/mediawiki/dnaa>.
- 836 [56] Hopcroft J, Tarjan R (1973) Algorithm 447: efficient algorithms for graph manipulation. *Commun ACM* 16: 372–378.
- 838 [57] Lunter G, Goodson M (2011) Stampy: a statistical algorithm for sensitive and fast mapping of illumina sequence reads. *Genome research* 21: 936–939.
- 840 [58] Li H (2011) A statistical framework for SNP calling, mutation discovery, association mapping and population genetical parameter estimation from sequencing data. *Bioinformatics* 27: 2987–2993.
- 842
- [59] Yang Z (1996) Statistical properties of a DNA sample under the finite-sites model. *Genetics* 144: 1941–1950.
- 844
- [60] Haldane JBS (1919) The combination of linkage values and the calculation of distances between the loci of linked factors. *Journal of Genetics* 8: 299–309.
- 846
- [61] Gordon D, Abajian C, Green P (1998) Consed: a graphical tool for sequence finishing. *Genome research* 8: 195–202.
- 848
- [62] Slater GS, Birney E (2005) Automated generation of heuristics for biological sequence comparison. *BMC Bioinformatics* 6: 31.
- 850
- [63] Edgar RC (2004) MUSCLE: multiple sequence alignment with high accuracy and high throughput. *Nucleic Acids Research* 32: 1792–1797.
- 852
- [64] Ronquist F, Huelsenbeck JP (2003) MrBayes 3: Bayesian phylogenetic inference under mixed models. *Bioinformatics* 19: 1572–1574.
- 854
- [65] Yang Z, Nielsen R (2000) Estimating synonymous and nonsynonymous substitution rates under realistic evolutionary models. *Molecular Biology and Evolution* 17: 32–43.
- 856
- [66] Zhang Z, Li J, Zhao XQ, Wang J, Wong GKS, et al. (2006) KaKs calculator: Calculating ka and ks through model selection and model averaging. *Genomics, Proteomics & Bioinformatics* 4: 259–263.
- 858
- [67] Benaglia T, Chauveau D, Hunter R David, Young S Derek (2009) mixtools: An r package for analyzing finite mixture models. *Journal of Statistical Software* 32: 1–29.
- 860
- 862

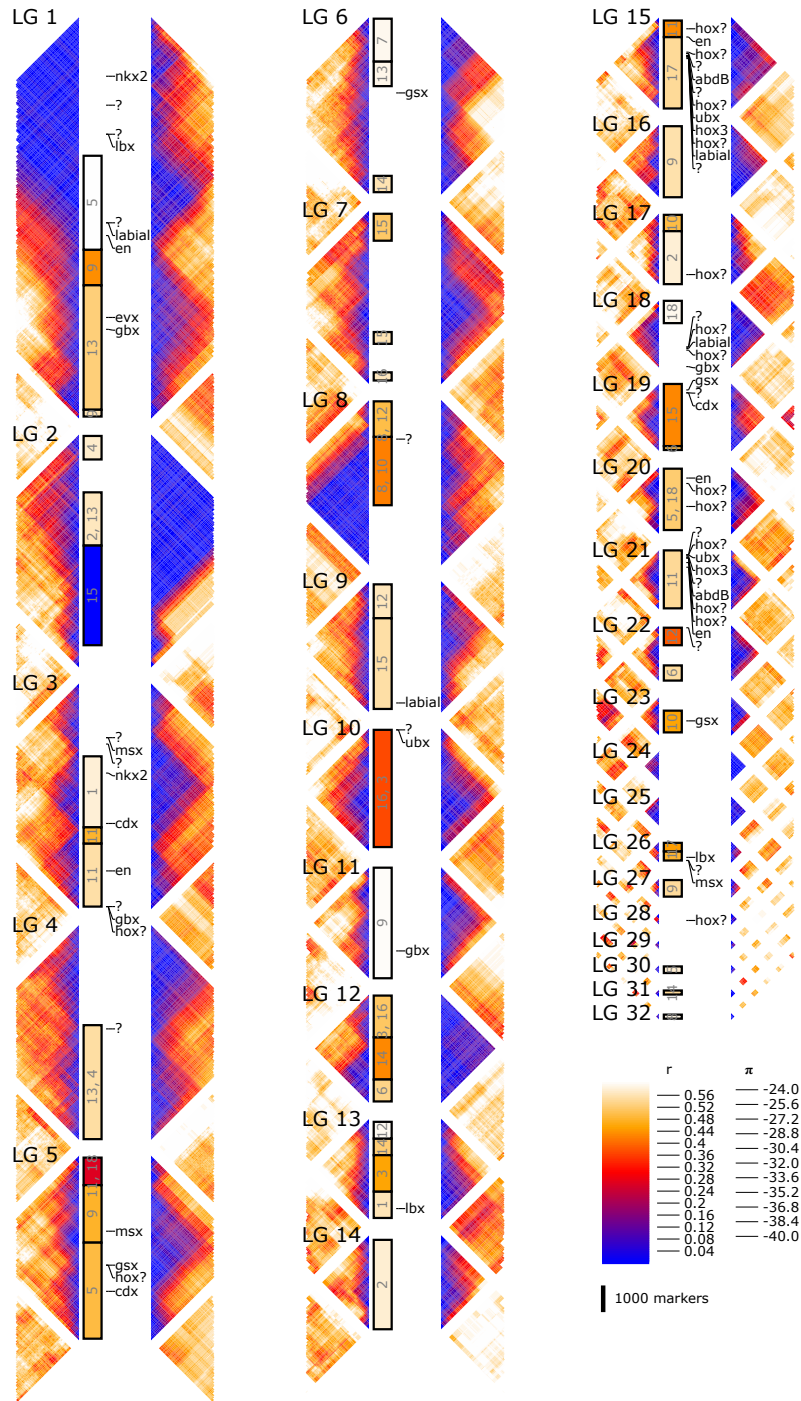


Figure 3: Each of the numbered blocks represents one of the 32 linkage groups of the *L. polyphemus* genetic map, and is composed of four columns: Two bands of the triangular matrices in which the color scale indicates the fraction of samples showing recombination between pairs of markers; maternal recombination frequency is shown on the left, paternal on the right. A column labeled "ALG" indicates segments of significant ($p < 0.05$ in Fisher's Exact Test, after Bonferroni correction for multiple tests) conservation of gene content with ancestral bilaterian lineage groups. The column labeled HOX shows the map positions and types of predicted homeobox transcription factor genes. The two color scales are for: recombination frequency between pairs of markers and log p-value for enrichment in gene content with ancestral linkage groups.

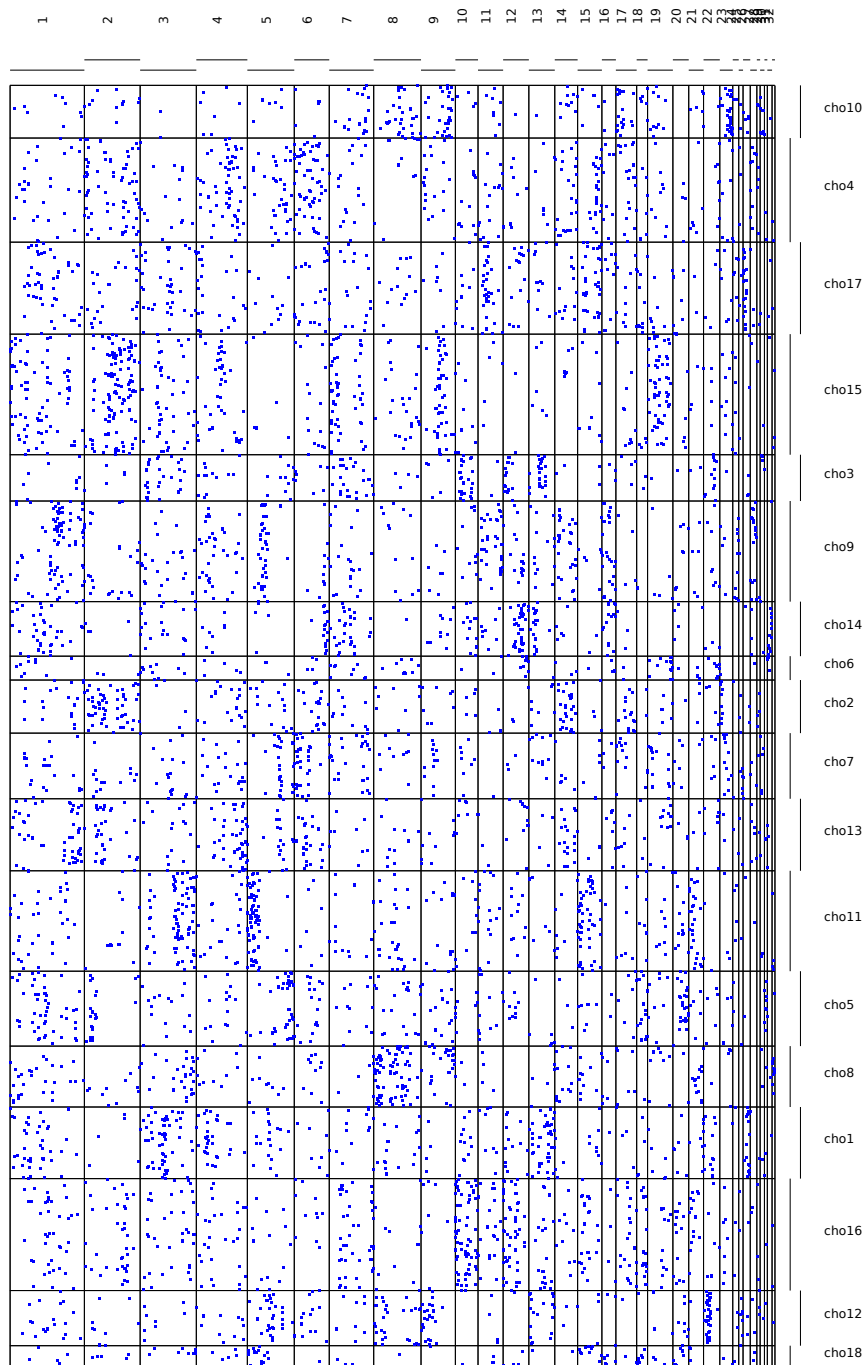


Figure 4: Limulus-Human macro-synteny dot plot. Blue points indicate the position of human genes in reconstructed ancestral chordate ALGs (vertical displacement) and their candidate orthologs in the 30 *L. polyphemus* linkage groups (horizontal displacement).

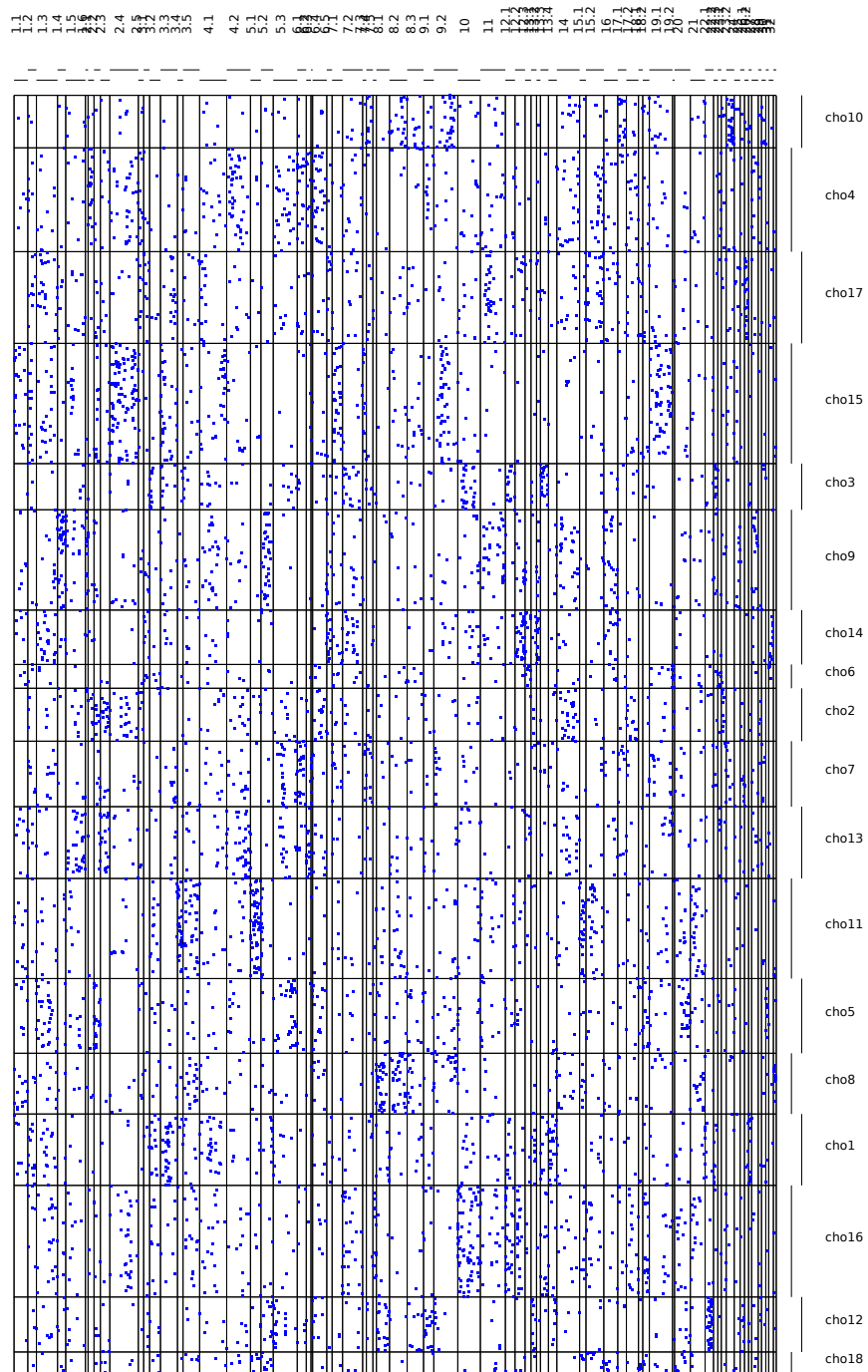


Figure 5: Limulus-Human macro-synteny dot plot as in Figure 4, showing breaks introduced by hidden Markov model segmentation of the linkage groups as vertical lines.

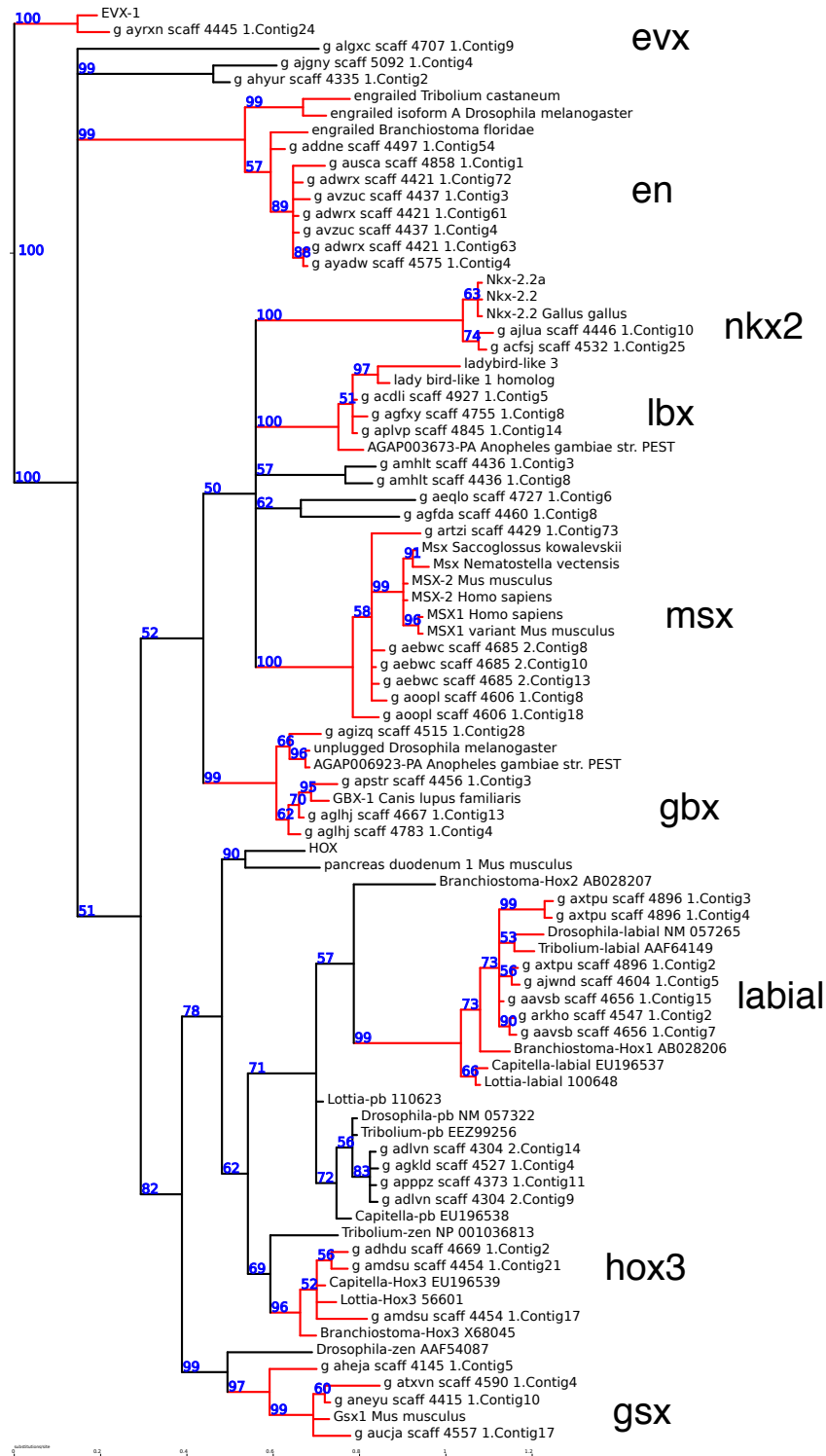


Figure 6: Unrooted phylogenetic tree of homeobox sequences (part 1). Nodes are labeled with Bayesian posterior probabilities. Highly supported partitions used to classify *L. polyphemus* sequences are drawn in red, with the abbreviation for the class shown in large letters. *L. polyphemus* homeobox sequences not grouped into one of these highly supported partitions are assigned to class "?". For ease of display, a large subtree consisting of HOX and parahox genes has been pruned at the position labeled "HOX", and is shown in Figure 7.

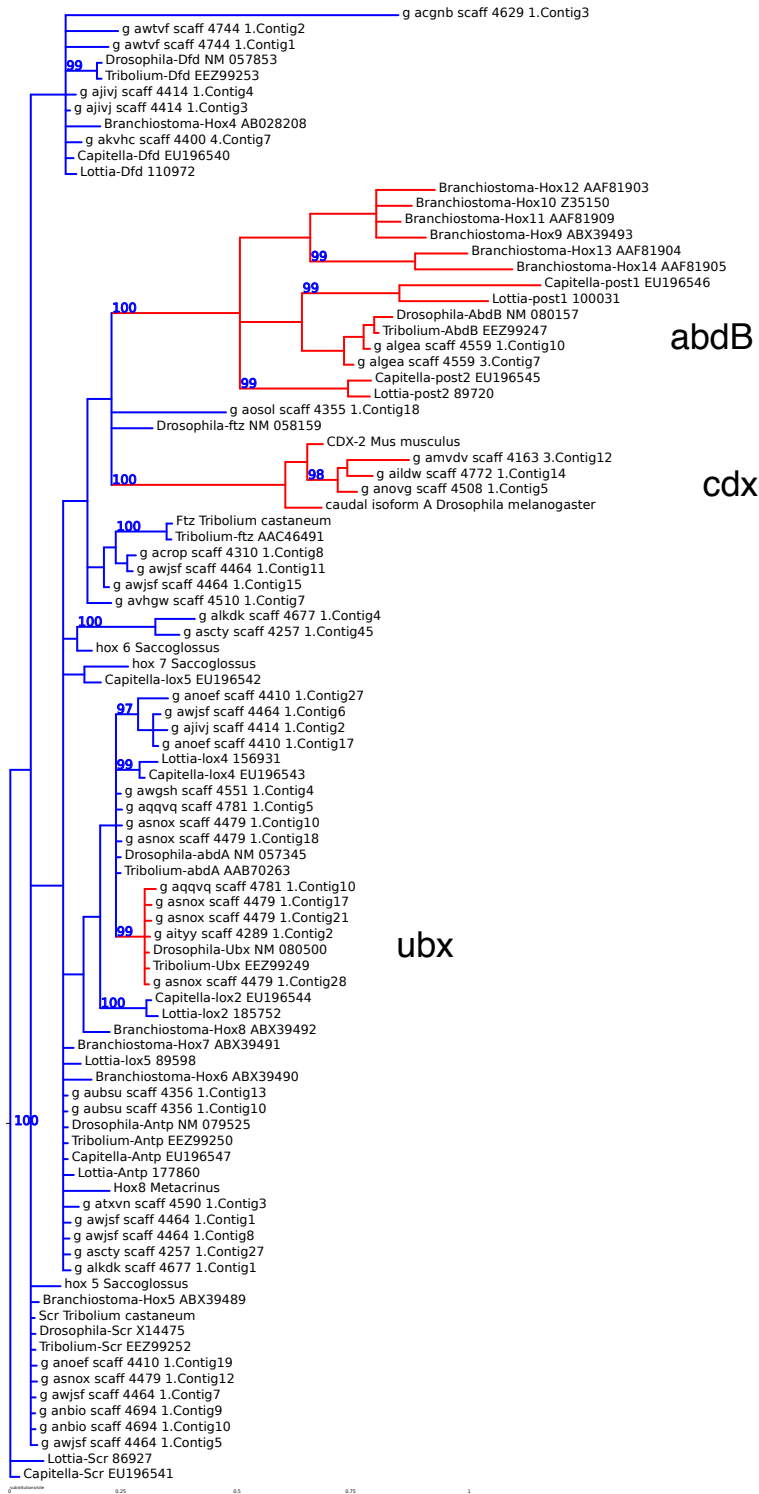


Figure 7: Phylogenetic tree of homeobox sequences, part 2. The rooted subtree pruned from the tree in Figure 6. Nodes are labeled with Bayesian posterior probabilities. Highly supported partitions used to classify *L. polyphemus* sequences are drawn in red, with the abbreviation for the class shown in large letters. *L. polyphemus* homeobox sequences not grouped into one of these highly supported partitions are assigned to class “hox?”.

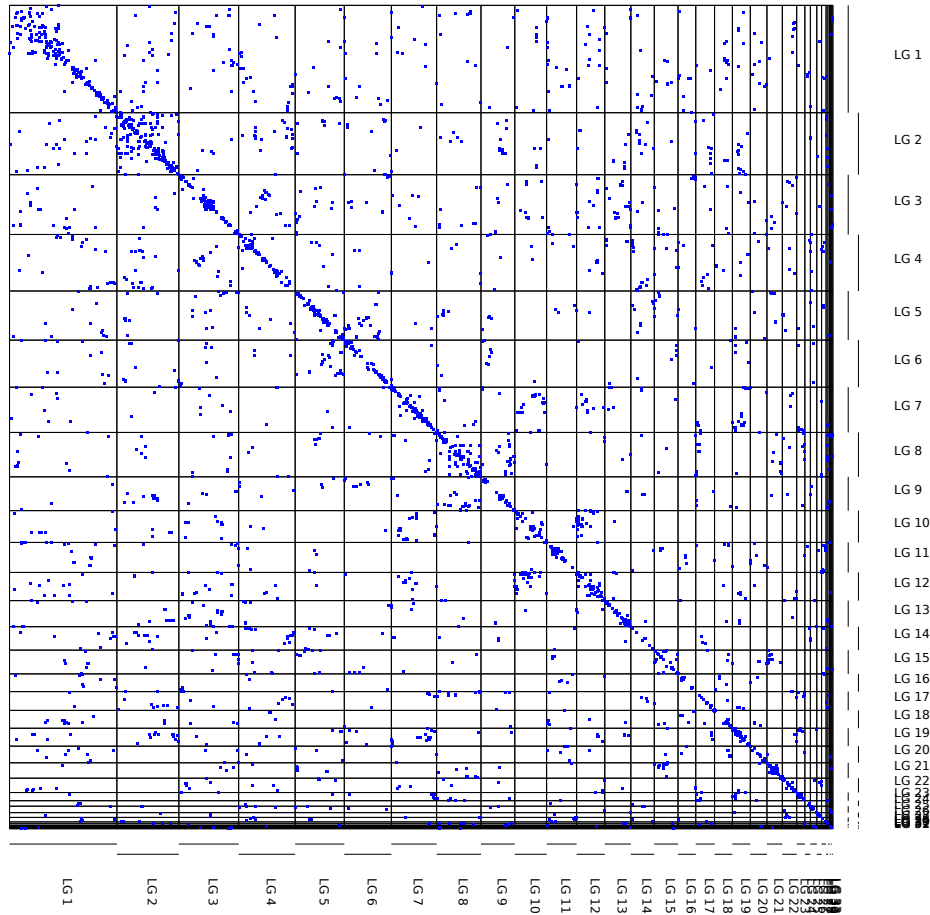


Figure 8: Genomic distribution of candidate paralogs

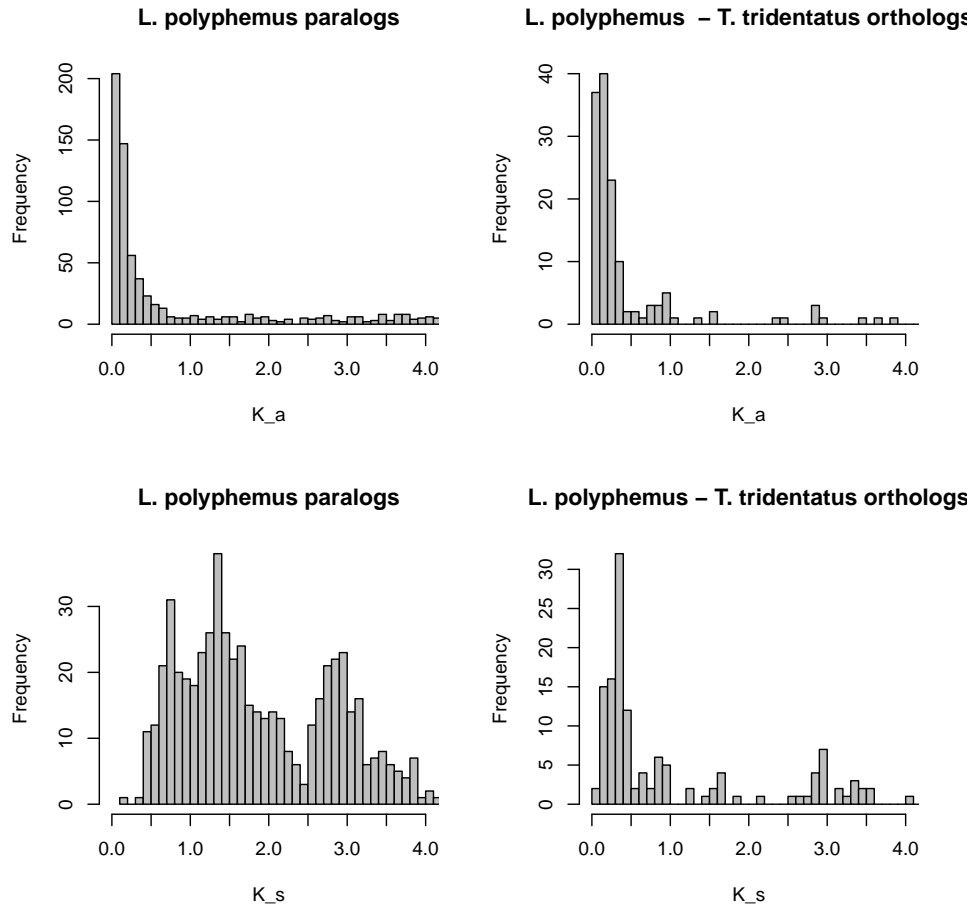


Figure 9: Distribution of synonymous and non-synonymous sequence divergence rates for pairs *L. polyphemus* paralogs and *L. polyphemus* - *T. tridentatus* orthologs.

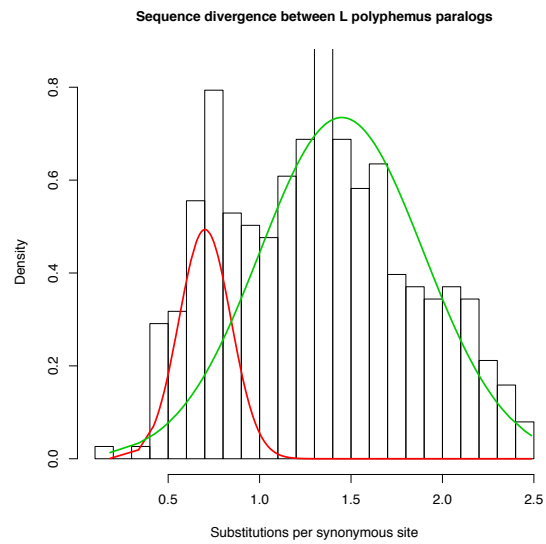


Figure 10: Two component mixture model fit to the K_s peak on the range $0 \leq K_s \leq 2.5$.